

## Directed Growth of Silk Nanofibrils on Graphene and Their Hybrid Nanocomposites

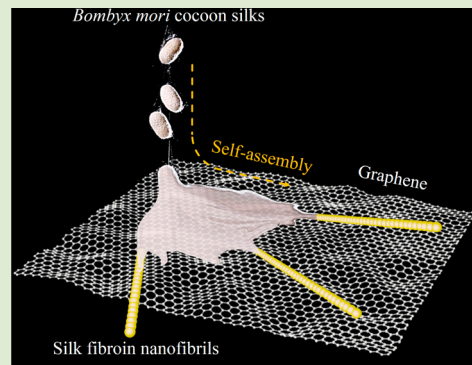
Shengjie Ling,<sup>†,‡</sup> Chaoxu Li,<sup>†</sup> Jozef Adamcik,<sup>†</sup> Suhang Wang,<sup>‡</sup> Zhengzhong Shao,<sup>‡</sup> Xin Chen,<sup>\*,‡</sup> and Raffaele Mezzenga<sup>\*,†</sup>

<sup>†</sup>Food and Soft Materials Science, Institute of Food, Nutrition and Health, ETH Zürich, LFO23, Schmelzbergstrasse 9, 8092 Zürich, Switzerland

<sup>‡</sup>State Key Laboratory of Molecular Engineering of Polymers, Department of Macromolecular Science, Laboratory of Advanced Materials, Fudan University, Shanghai, 200433, People's Republic of China

### Supporting Information

**ABSTRACT:** Combination of proteins with other nanomaterials offers a promising strategy to fabricate novel hybrids with original functions in biology, medicine, nanotechnology, and materials science. Under carefully selected experimental conditions, we show that graphene nanosheets are able to direct one-dimensional self-assembly of silk fibroin, forming an unprecedented type of nanohybrids. These silk/graphene hybrids combine physical properties of both constituents and form functional composites with well-ordered hierarchical structures. Due to the facile fabrication process and their tunable nanostructures, the resultant hybrids show promise in applications as diverse as tissue engineering, drug delivery, nanoelectronics, nanomedicine, biosensors, and functional composites.



Self-assembly of proteins has been intensively studied in the past few decades as a fundamental strategy to build hierarchical structures in both living systems and novel advanced materials for bionanotechnology purposes.<sup>1–3</sup> In particular, the possibility of intercalating in between protein layers with other molecules or nano-objects at subnanometer length scales resolution, opens unprecedented opportunities to construct zero to three-dimensional proteinaceous hybrids with exceptional structures and functions suitable in medical/biological applications. For example, considerable effort has been devoted to utilize protein assemblies to induce/template the growth of inorganic materials, in analogy with the formation of natural bone, enamel, eggshell, and nacre.<sup>4–6</sup> In sharp contrast, the opposite, that is, how inorganic/synthetic nanomaterials can induce the growth and organization of protein assemblies, remain much less understood and investigated. For example, only recently has the role of graphene nanosheets in directing protein and peptide self-assembly started to emerge.<sup>7</sup> This remains, however, a challenging subject because of the difference in solubility among the two species as well as the restricted window of processing conditions, which can be applied to these materials together. Nevertheless, by carefully selecting functional nanomaterials and proteins, their combination can be efficiently engineered into the production of hybrids with unprecedented structures and properties.

Graphene nanosheets are ideally suitable in the present study not only because of their unique aspect ratio, yielding a truly 2D geometric architecture, but also due to their extraordinary

physical and chemical stability, as well as thermal, mechanical, and optoelectronic properties.<sup>8,9</sup> Despite their demonstrated applicability in biosensors, drug delivery, cell detection, and cell imaging,<sup>9</sup> their potential in bionanotechnology remains somehow underestimated due to disadvantages such as highly hydrophobic, featureless surfaces, low aqueous solubility, and lack of biocompatibility.<sup>10</sup> To overcome these disadvantages, many natural biomacromolecules (e.g., DNA and proteins) have been bound on the surfaces of graphene nanosheets,<sup>7,10–12</sup> although the low coverage resulting from the exceptionally high aspect ratio of graphene has allowed addressing only part of the issues.<sup>13</sup> Because graphite, the stacking form of graphene nanosheets, has shown a strong templating effect for protein assembly,<sup>13–15</sup> it is nonetheless expected that fully exfoliated graphene nanosheets shall be capable of directing the growth of protein assemblies in a rather unique way.

Animal silks (mainly spider and silkworm silks) are known to be one of the strongest natural biomaterials.<sup>16</sup> Besides, low cost and availability of silk fibroin (SF), a protein derived from *Bombyx mori* (*B. mori*) silkworm cocoons, make it a very attractive protein material in both the academic and industrial fields.<sup>17–19</sup> It has been found that SF has excellent biocompatibility as well as tunable degradability.<sup>18,19</sup> Therefore, SF has been frequently mineralized<sup>20–22</sup> or combined with

**Received:** December 17, 2013

**Accepted:** January 13, 2014

**Published:** January 14, 2014

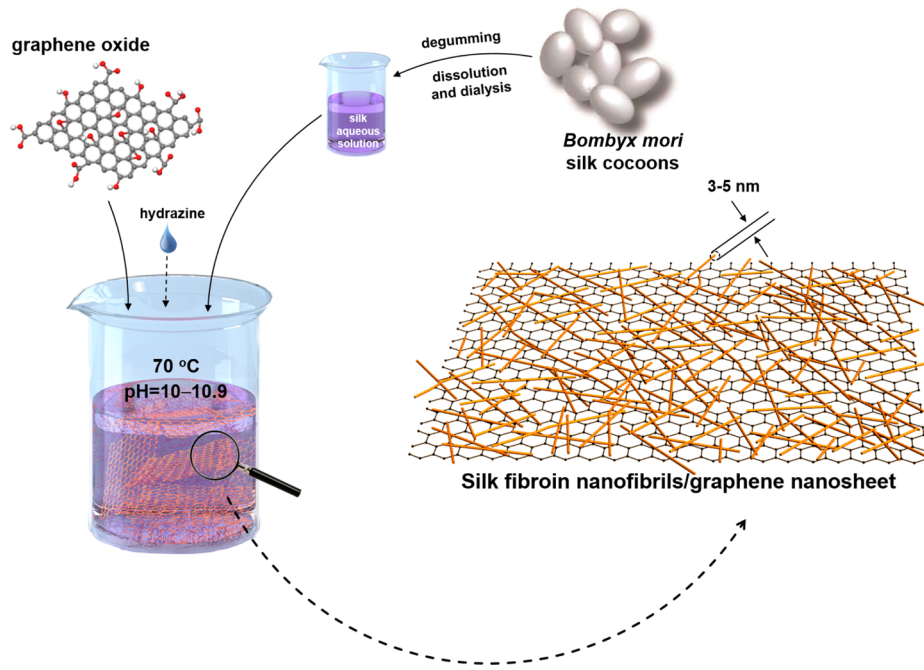


**Figure 1.** Schematic representation of the procedure followed to prepare SF nanofibril/graphene hybrids. SF solution (5 wt %) was prepared from *B. mori* silkworm cocoons. Graphene oxide and SF solutions were mixed at various mass ratios and incubated at 70 °C and pH = 10–10.9 for 6 h in the presence of hydrazine.

other materials to produce high-performance hybrids.<sup>23–25</sup> Nonetheless, although the mechanical properties of natural spider and engineered silk are well-recognized,<sup>16,26</sup> the control on the self-assembly and structural complexity of SF during processing is still far from being entirely understood.<sup>27–31</sup> The majority of previous attempts have focused on the changes in secondary structures during the spinning process of silk macrofibers.<sup>1,26</sup> There are only a few reports that have tackled the hierarchical self-assembly of SF at all the relevant length scales,<sup>28–31</sup> but to the best of our knowledge, no report has yet studied the directed growth of SF assemblies in the presence of a graphene nanosheet.

In this study we show that unbranched SF nanofibrils can grow, preferentially and efficiently, on graphene nanosheets under a specific window of experimental conditions (pH, mass ratio, concentration, and temperature). First, these findings confirm that exfoliated graphene nanosheets are able to direct the growth of protein assemblies. Second, differently from other studies where only a limited coverage of graphene nanosheets by individual adhering molecules was demonstrated,<sup>7,10–12</sup> in the present case, a nearly entire coverage of graphene nanosheets by SF assemblies is shown, which immediately translates into superior aqueous solubility compared to previous reports, but also into more readily available functional groups on the surfaces, controllable mechanical flexibility, and enhanced biocompatibility, opening a new opportunity for graphene processing and applications.<sup>10</sup> Third, self-assembly of SF on a graphene surface also provides the possibility of shedding new light into the roles of hydrophobic interactions with respect to protein assembly. Finally, we show how the resultant hybrids can be used to produce nanocomposites with remarkable mechanical properties, perfectly organized hierarchical structures, and enhanced biocompatibility, allowing their use as cellular growth scaffolds and, thus, expanding the range of applications of graphene in medical/biological fields.

The assembly approach followed to generate the hybrids is sketched in Figure 1. First, *B. mori* silkworm cocoon silk fibers were degummed, dissolved and dialyzed in accordance with a typical protocol described in available literatures<sup>21,22,26</sup> and Supporting Information, yielding a solution of protein concentration of about 5 wt %. The solution was further adjusted to 0.1 wt % and a given (variable) pH and then mixed with the desired amount of graphene oxide (GO) solution, which was synthesized following a modified Hummers method (Supporting Information).<sup>32</sup> Due to the existence of an isoelectric point (pI) of 4.53,<sup>33</sup> SF was negatively charged at basic pH as GO. Consequently, a homogeneous suspension was obtained upon moderately stirring. After adding 50 μL hydrazine, the suspension was incubated at 70 °C for 6 h to reduce GO into graphene<sup>34</sup> in the presence of silk proteins. The resultant graphene nanosheets can be fully exfoliated while getting covered by amphiphilic SF molecules. This is confirmed by the set image in Figure 2a, corresponding to an atomic force microscopy (AFM) image from a solution prepared with 8:2 SF/graphene ratio at pH 10.3. The black homogeneous suspension is stable up to 6 months without precipitation. However, instead of single layer of protein molecules,<sup>35,36</sup> we found that graphene was covered by layers of densely packed nanofibrils (see Figures 2a and S1a). It should be emphasized that the reduction of GO and the assembly of protein nanofibrils took place simultaneously in this incubation single-step process. Further transmission electron microscopy (TEM) and AFM analysis reveal that there are only a few SF nanofibrils observed outside graphene (over 10<sup>2</sup> times less dense comparing to the density observed on graphene surfaces), indicating the nanofibrils are selectively present on graphene nanosheets only (Figure S2). In addition, we found SF nanofibrils could also grow on graphene nanosheet without the addition of hydrazine (Figure S3) but needed a prolonged incubation time (for instance, from 6 to 24 h at the same condition of Figures 2a and S1a). It has already been reported

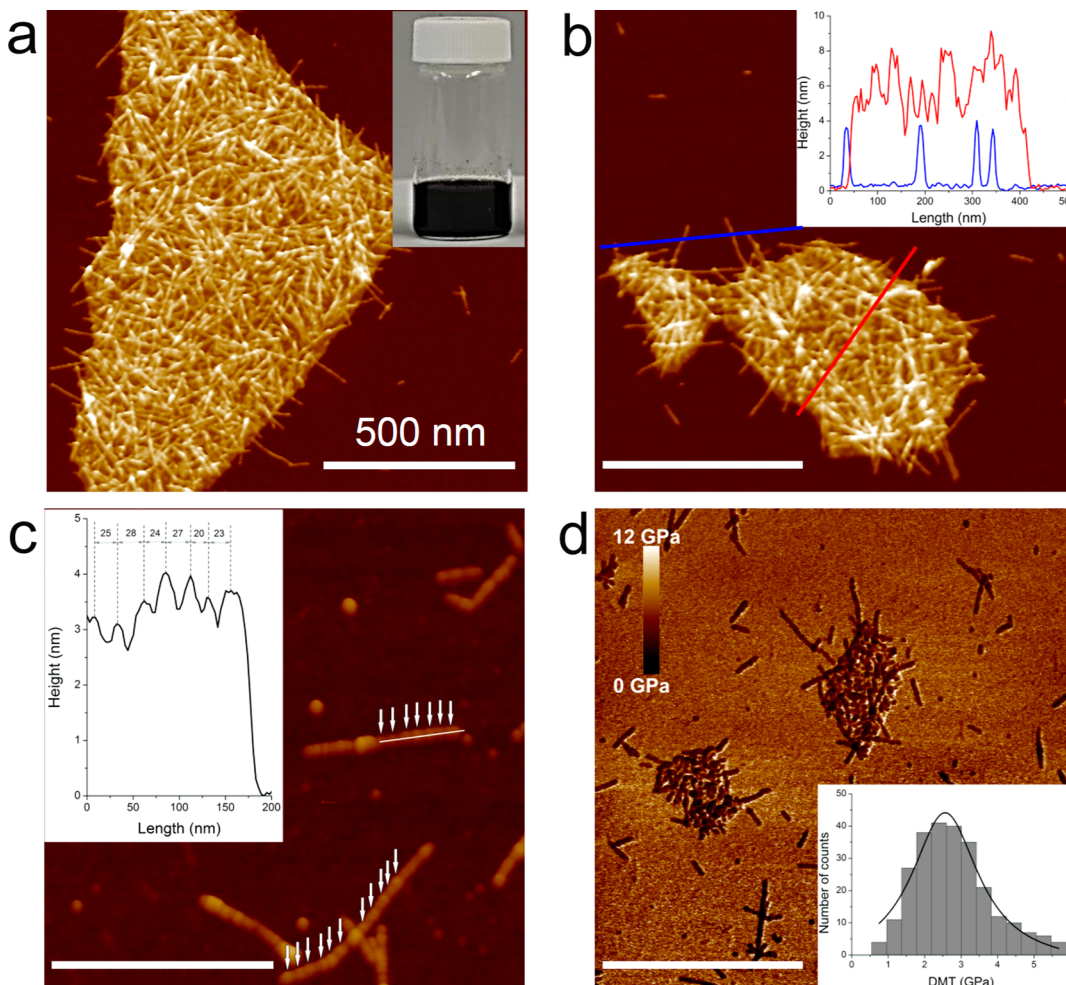


**Figure 2.** Structural characterization of SF nanofibril/graphene hybrids. (a) AFM image of the hybrid prepared from SF/graphene (8:2) at pH 10.3. The inset shows that the hybrid solution remains stable for several months. (b) AFM image with height profiles collected along the indicated colored lines. (c) Height profile along the contour length nanofibrils prepared from SF/graphene (5:5) at pH 10.3, highlighting the necklace structure of the nanofibrils. (d) DMT moduli image of the hybrids prepared from SF/graphene (8:2) at pH 10.3. The inset refers to the DMT modulus distribution of the nanofibrils measured on top of a single graphene sheet. All scale bars in images are 500 nm.

that SF is also able to reduce GO to graphene,<sup>36</sup> and obviously the reducing ability of SF is much weaker than hydrazine.

Structural details of the SF nanofibrils are provided by following the height profiles collected along the indicated AFM traces. The SF nanofibrils have a height of  $3.5 \pm 0.5$  nm (see the blue curve in the inset of Figure 2b) and a contour length in the range of 300–500 nm. The red curve in the inset of Figure 2b shows that the height can reach up to 9 nm, indicating SF nanofibrils grow on the double-sided graphene sheet (single height of SF nanofibril is 3.5 nm plus around 1 nm thickness of graphene sheet). Careful examination reveals that the SF nanofibrils have a necklace-like morphology (see Figure S1b). The center-to-center distance of the beads is  $25 \pm 3$  nm indicated along an individual nanofibril outside graphene in Figure 2c, similar to the nanofibrils found in natural spider silk fibers.<sup>18,37</sup>

Considering the high modulus of natural silk fibers,<sup>38,39</sup> we set out to investigate the mechanical properties of these SF nanofibrils by extracting them via nanoindentation in AFM, following a Derjaguin–Mueller–Toporov (DMT) mode described in our previous reports.<sup>40,41</sup> As shown in Figure 2d, the SF nanofibrils have an average DMT modulus of 2.5 GPa, which is comparable with the fibril moduli of chitin and

collagen.<sup>42</sup> More in general, other types of  $\beta$ -sheet based fibrils, that is, the amyloid fibrils, are also reported to have a modulus in the range of 2–5 GPa.<sup>40,41</sup>

Both the presence of graphene and processing conditions proved to be key to generate the observed self-assembly: by setting the starting pH to 10.86 and incubating at 70 °C, no nanofibrils are found in the absence of graphene (Figure S4a), while in the presence of graphene, the nanosheets are found to be fully covered by short SF nanofibrils (Figure S4b). This finding convincingly proves that graphene has a crucial role in the formation of SF nanofibrils. To further rule out the possibility that the growth of the SF nanofibrils occurs independently from the presence of graphene and it is simply a result of adsorption, we run additional control experiments by decreasing the pH to 10.5 (within the nanofibril formation window), then forming SF nanofibrils without graphene (Figure S4c), and adding graphene afterward. Under these conditions only a few SF nanofibrils could be observed on graphene nanosheets, AFM and TEM providing identical results (Figure S4d and S4e), confirming that the saturation of SF nanofibrils on top of graphene nanosheets, as shown in Figure 2a,b, is not the result of simple adsorption, but rather of a specific in situ nanofibrils growth.

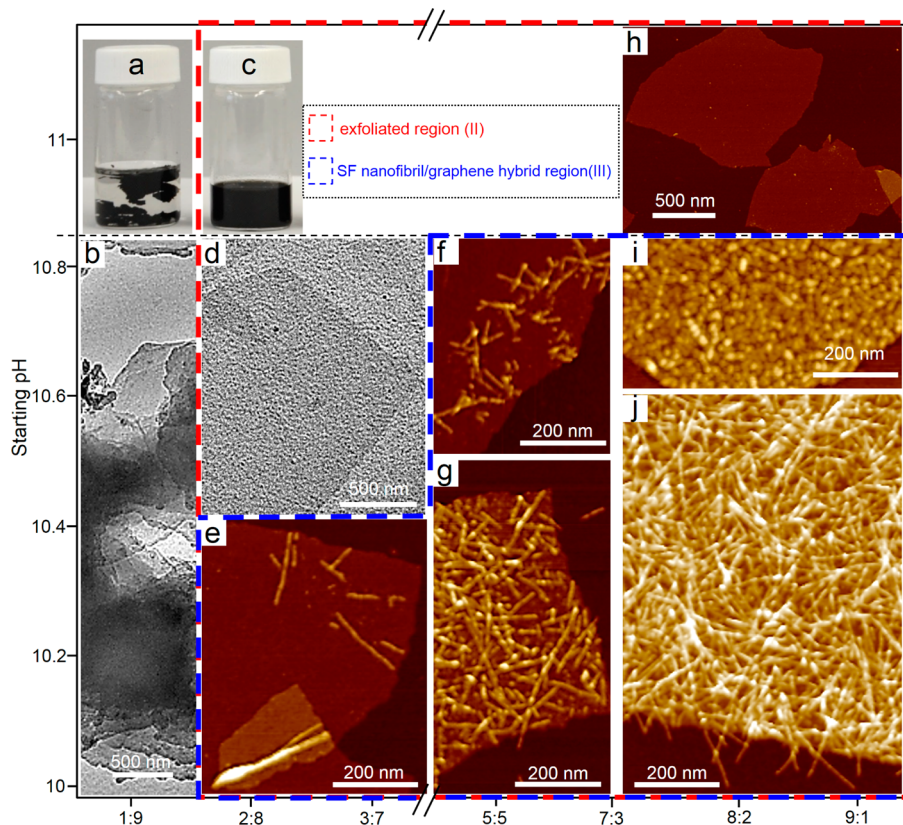


**Figure 3.** Dependence of SF assembling behavior on both pH and SF/graphene mass ratio. Exfoliated regions and SF nanofibril/graphene hybrid regions were indicated as red and blue boxes, respectively. Photographs of final suspensions with SF/graphene ratio 1:9 (a) and 2:8 (c) ratios at pH 10.5. (b) TEM image of the suspension in (a). (d) TEM image of the hybrid with 3:7 SF/graphene ratio at pH 10.6. (e) AFM image of the hybrid with 3:7 SF/graphene ratio at pH 10.3. (f, g) AFM images of the hybrid with 5:5 SF/graphene ratio at pH 10.7 and 10.3, respectively. (h–j) AFM image of the hybrid with 8:2 SF/graphene ratio at pH 11, 10.8, and 10.3, respectively.

The directed assembly of SF nanofibrils on graphene in this study may closely link to its pure  $sp^2$ -hybridized carbon surfaces. Due to the presence of hydrophobic interactions with nonpolar moieties of the proteins, it has been reported before that graphite surfaces may adsorb protein monomers and oligomers, thus, promoting the formation of  $\beta$ -sheets and templating amyloid fibrillation.<sup>13</sup> In contrast, by oxidizing graphite into GO, the existence of multiple hydrophilic functional groups was shown to inhibit amyloid fibrillation.<sup>43</sup> Bearing a surface chemical analogue to that of graphite, but with the much higher specific surface area of about  $2600\text{ m}^2/\text{g}$ , graphene nanosheets are thus expected to promote the formation of SF nanofibrils, which are constituted by chains containing alternating hydrophobic and hydrophilic blocks. The hydrophobic blocks consist of highly conserved sequences of the repeat motif GAGAGS that are known to form anisotropic  $\beta$ -sheets.<sup>18,44</sup> The  $\beta$ -sheet based structure similarity between amyloid fibrils and silk nanofibrils also supports our hypothesis.<sup>45,46</sup> Compared with the conventional ethanol-treated SF film, not only shows the hybrid nanocomposites (with 7:3 SF/graphene ratio) pronounced silk I X-ray scattering peaks at  $1.35$  and  $1.7\text{ \AA}^{-1}$  (characteristic of a  $\beta$ -turn type II-like structure), but also exhibits a much stronger silk II peak at  $1.4\text{ \AA}^{-1}$ , corresponding to the antiparallel  $\beta$ -sheet structure with  $d$  spacing at  $4.5\text{ \AA}$ ,<sup>47</sup> which indicated that SF nanofibrils are richer in  $\beta$ -sheets than ethanol-treated SF film, shown in Figure S5a.

The dependence of SF assembling on both the starting pH and SF/graphene mass ratio is shown in Figure 3. The pH value

was restricted above pH 10, because neutral SF is well-known to rapidly denature into insoluble aggregates at lower pH and high enough temperatures. Three distinct regions can be identified in Figure 3: (I) unstable region, (II) exfoliated graphene region, and (III) SF nanofibril/graphene hybrids region. In region I, the amount of SF is not sufficient to stabilize the reduced graphene, which sediments quickly after stopping stirring (see Figure 3a,b). In region II, graphene nanosheets are fully exfoliated (see Figure 3c,d,h) due to the amphiphilic properties of SF as well as its negative charges ( $pI = 4.53$ ):<sup>33</sup> with enough SF molecules being attached on graphene nanosheets, they gain the needed electrostatic repulsion to be stabilized.<sup>35,36</sup> In region III, graphene nanosheets were densely covered by SF nanofibrils. We found that the covering density and contour length of the nanofibrils could be controlled by varying the processing parameters. For example, the covering density can be controlled by varying the SF/graphene mass ratio. An increase in covering density from about 5% to about 95% is shown in Figure 3e,j. The contour length of nanofibrils was tuned by changing the starting pH. For an example, a length of  $300\text{--}500\text{ nm}$  in Figure 3g,j jumps to  $5\text{--}80\text{ nm}$  in Figure 3f,i when the pH increases from 10.3 to 10.8.

The findings above show how graphene can be functionalized with SF nanofibrils in a simple one-step incubation process. The resulting hybrids combine physical properties of both the graphene and SF. To fabricate macroscopic materials, we followed a simple vacuum filtration process as reported

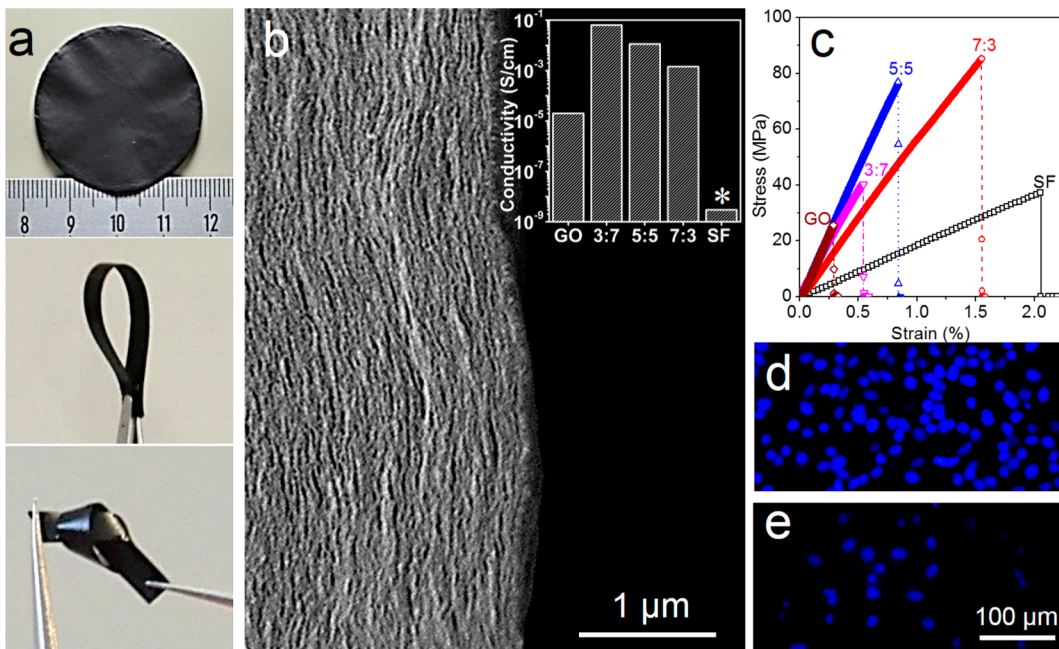


**Figure 4.** Physical characterization of macroscopic hybrid films. (a) Photograph of free-standing SF nanofibrils/graphene composite. (b) SEM image of the film with 8:2 SF/graphene ratio. The inset gives the dependence of the conductivity on SF/graphene ratio. The symbol \* for silk stands for the insulating nature of pure SF nanofibrils whose electrical conductivity is below the detection range of  $10^{-8}$  S cm $^{-1}$ . (c) Tensile properties of the films. (d, e) Comparison of fluorescence image of HeLa cells growing for 3 days on the film with 8:2 SF nanofibrils/graphene ratio (d) and 100% graphene (e).

previously.<sup>10,48</sup> The resulting free-standing films (about 20  $\mu$ m thick) are flexible and can easily undergo bending and knotting (see Figure 4a), even when the silk composition gets as low as 30 wt %. This is remarkable because most filtration-based graphene composites lack flexibility, either due to a high graphene content or due to low flexibility of the constituents.<sup>48</sup> SEM analysis reveals a well-organized layered structure even when the nanocomposites contain 80 wt % SF (Figure 4b), in which the high SF content is not found to perturb the ordered organization. Importantly, the structure and morphology of films show excellent uniformity and reproducibility.

The combination of graphene with SF also provides the nanocomposites with tunable in-plane conductivity (inset plot in Figure 4b). An electric conductivity of  $1.4 \times 10^{-3}$  to  $1.1 \times 10^{-2}$  S cm $^{-1}$  was achieved depending on the SF content, which is over 2 orders of magnitude larger than pure GO and comparable with other examples of graphene films with similar structure and content of insulating constituent.<sup>10,49,50</sup> In contrast, pure SF nanofibrils are insulating, with an electric conductivity below  $10^{-8}$  S cm $^{-1}$ . The mechanical analysis shows that graphene reinforced SF materials (Figures 4c and S5). The hybrids have tensile modulus of 6–10 GPa that is at least 4 times larger than that of silk films (about 1.5 GPa) and compare well with other graphene papers reported in the literature.<sup>10,50</sup> As far as toughness is concerned, the hybrids films have values of  $3 \times 10^5$ – $6 \times 10^5$  J/m $^3$  (SF nanofibrils/graphene ratio 5:5–7:3), over 10× higher than that of pure GO (Figure S5), producing a tougher graphene composite material. As a comparison, films made of pure amyloidogenic protein fibrils, such as  $\beta$ -lactoglobulin, easily break on normal handling, unless they have also been blended with graphene<sup>10</sup> or other inorganic nanoparticles.<sup>51</sup> We finally show that the composites have excellent biocompatibility and can be used as scaffolds for cell growth. As shown in Figure 4d, HeLa cells, a commonly

used cell line, were grown on the films. The cells showed excellent adhesion on 8:2 SF nanofibrils/graphene nanocomposites (Figure 4d). After 72 h of culture time, the fluorescent area is 5 times larger than what observed for the same cell lines growth under identical conditions on pure graphene (Figure 4e), which demonstrates the presence of metabolically active cells on the nanocomposite.

In summary, we prepared a new type of hybrid nanocomposite via a facile one-step protocol, where SF nanofibrils preferentially grow on graphene surfaces. The SF nanofibrils have a modulus comparable with that of amyloid fibrils, chitin fibrils, and collagen fibrils<sup>40–42</sup> and can be engineered within a broad range to adjust their contour length and coverage of graphene nanosheets. By simply using a vacuum-assisted filtering process, these colloidal hybrids can be processed into well-structured macroscopic films, which have excellent physical properties combining features from both graphene and silk. These hybrids may prove useful (templating protein assemblies with nanomaterials) in designing advanced materials of use in tissue engineering, nanoelectronics, biosensors, and functional composites.

## EXPERIMENTAL SECTION

The SF aqueous solution was prepared from *B. mori* silkworm cocoons followed a well-established procedure,<sup>26</sup> including degumming, dissolving, and dialysis. The dialyzed SF solution was centrifuged at 6000 r/min for about 5 min to remove insoluble part. The final concentration of the SF aqueous solution was 5 wt %. The GO was synthesized using a modified Hummers method<sup>32</sup> (see Supporting Information).

Desired quantities of SF solution (pH = 7) and Millipore water were dropped simultaneously into the GO solution under vigorous stirring to give a final mixture (30 mL) with a GO concentration of 0.1 wt % and solid mass ratios of 1:9, 2:8, 3:7, 5:5, 7:3, 8:2, and 9:1 for GO/SF. After adjusting the pH with 1.0 mol L $^{-1}$  NaOH, 50  $\mu$ L

hydrazine monohydrate was added into the mixture as reducing agent for GO. Afterward, the GO/SF mixture was incubated at 70 °C for 6 h.

The SF nanofibrils/graphene composites were fabricated by vacuum filtration of the suspensions prepared above using a Sigma-Aldrich vacuum filtration assembly and nylon filtration membranes (pore size, 0.2 mm; diameter, 47 mm; Sigma-Aldrich). Film thickness was controlled by the solution volume being filtered.

**Characterization.** The hybrids were characterized by TEM (Philips TEM CM 20) and AFM (Nanoscope VIII, Bruker, U.S.A.). Morphology and structure of the films were characterized by SEM and WAXS. Mechanical properties were tested by using an electronic-controlled tensile apparatus. Conductivity measurements were performed by using HMS-3000 Hall Measurement System with four-point probes. Biocompatibility test was performed by monitoring the growth of Hela cells on the hybrid nanocomposites. The cells were stained with 4',6'-diamidino-2-phenylindole (DAPI). Additional details are provided in the Supporting Information.

## ■ ASSOCIATED CONTENT

### Supporting Information

Preparation of silk protein solution, synthesis of graphene oxide, AFM, TEM, and SEM characterization, conductivity measurements, WAXS/SAXS, and growth of Hela cells. This material is available free of charge via the Internet at <http://pubs.acs.org>.

## ■ AUTHOR INFORMATION

### Corresponding Authors

\*E-mail: chenx@fudan.edu.cn.

\*E-mail: raffaele.mezzenga@hest.ethz.ch.

### Notes

The authors declare no competing financial interest.

## ■ ACKNOWLEDGMENTS

This work is supported by the China Scholarship Council, the National Natural Science Foundation of China (Nos. 20974025, 21034003), the National High Technology Research and Development Program of China (863 Program; No. 2012AA030309), and ETH Zurich. We thank Dr. Antoni Sanchez-Ferrer at ETH Zurich and Dr. Jinrong Yao, Dr. Jianchuan Wen, and Yaxian Wang at Fudan University for their valuable suggestions and discussions.

## ■ REFERENCES

- (1) Vollrath, F.; Knight, D. P. *Nature* **2001**, *410*, 541–548.
- (2) Adamcik, J.; Mezzenga, R. *Macromolecules* **2012**, *45*, 1137–1150.
- (3) Cherny, I.; Gazit, E. *Angew. Chem., Int. Ed.* **2008**, *47*, 4062–4069.
- (4) Wang, Y.; Azais, T.; Robin, M.; Vallee, A.; Catania, C.; Legriel, P.; Pehau-Arnaudet, G.; Babonneau, F.; Giraud-Guille, M. M.; Nassif, N. *Nat. Mater.* **2012**, *11*, 724–733.
- (5) Nudelman, F.; Pieterse, K.; George, A.; Bomans, P. H. H.; Friedrich, H.; Brylka, L. J.; Hilbers, P. A. J.; de With, G.; Sommerdijk, N. A. J. M. *Nat. Mater.* **2010**, *9*, 1004–1009.
- (6) Carny, O.; Shalev, D. E.; Gazit, E. *Nano Lett.* **2006**, *6*, 1594–1597.
- (7) Han, T. H.; Lee, W. J.; Lee, D. H.; Kim, J. E.; Choi, E. Y.; Kim, S. O. *Adv. Mater.* **2010**, *22*, 2060–2064.
- (8) Georgakilas, V.; Otyepka, M.; Bourlinos, A. B.; Chandra, V.; Kim, N.; Kemp, K. C.; Hobza, P.; Zboril, R.; Kim, K. S. *Chem. Rev.* **2012**, *112*, 6156–6214.
- (9) Mao, H. Y.; Laurent, S.; Chen, W.; Akhavan, O.; Imani, M.; Ashkarran, A. A.; Mahmoudi, M. *Chem. Rev.* **2013**, *113*, 3407–3424.
- (10) Li, C. X.; Adamcik, J.; Mezzenga, R. *Nat. Nanotechnol.* **2012**, *7*, 421–427.
- (11) Patil, A. J.; Vickery, J. L.; Scott, T. B.; Mann, S. *Adv. Mater.* **2009**, *21*, 3159–3164.
- (12) Laaksonen, P.; Kainlahti, M.; Laaksonen, T.; Shchepetov, A.; Jiang, H.; Ahopelto, J.; Linder, M. B. *Angew. Chem., Int. Ed.* **2010**, *49*, 4946–4949.
- (13) Li, C. X.; Mezzenga, R. *Nanoscale* **2013**, *5*, 6207–6218.
- (14) Kowalewski, T.; Holtzman, D. M. *Proc. Natl. Acad. Sci. U.S.A.* **1999**, *96*, 3688–3693.
- (15) Brown, C. L.; Aksay, I. A.; Saville, D. A.; Hecht, M. H. *J. Am. Chem. Soc.* **2002**, *124*, 6846–6848.
- (16) Shao, Z. Z.; Vollrath, F. *Nature* **2002**, *418*, 741–741.
- (17) Omenetto, F. G.; Kaplan, D. L. *Science* **2010**, *329*, 528–531.
- (18) Hardy, J. G.; Scheibel, T. R. *Prog. Polym. Sci.* **2010**, *35*, 1093–1115.
- (19) Kaplan, D. L.; Vepari, C. *Prog. Polym. Sci.* **2007**, *32*, 991–1007.
- (20) Wang, T.; Porter, D.; Shao, Z. Z. *Adv. Funct. Mater.* **2012**, *22*, 435–441.
- (21) Fei, X.; Shao, Z. Z.; Chen, X. *J. Mater. Chem. B* **2013**, *1*, 213–220.
- (22) Fei, X.; Shao, Z. Z.; Chen, X. *Nanoscale* **2013**, *5*, 7991–7997.
- (23) Manoor, M. S.; Tao, H.; Clayton, J. D.; Sengupta, A.; Kaplan, D. L.; Naik, R. R.; Verma, N.; Omenetto, F. G.; McAlpine, M. C. *Nat. Commun.* **2012**, *3*, 763.
- (24) Hu, K. S.; Gupta, M. K.; Kulkarni, D. D.; Tsukruk, V. V. *Adv. Mater.* **2013**, *25*, 2301–2307.
- (25) Huang, L.; Li, C.; Yuan, W. J.; Shi, G. Q. *Nanoscale* **2013**, *5*, 3780–3786.
- (26) Zhou, G. Q.; Shao, Z. Z.; Knight, D. P.; Yan, J. P.; Chen, X. *Adv. Mater.* **2009**, *21*, 366–370.
- (27) Hagn, F.; Eisoldt, L.; Hardy, J. G.; Vendrely, C.; Coles, M.; Scheibel, T.; Kessler, H. *Nature* **2010**, *465*, 239–131.
- (28) Gong, Z. G.; Huang, L.; Yang, Y. H.; Chen, X.; Shao, Z. Z. *Chem. Commun.* **2009**, *48*, 7506–7508.
- (29) Gong, Z. G.; Yang, Y. H.; Huang, L.; Chen, X.; Shao, Z. Z. *Soft Matter* **2010**, *6*, 1217–1223.
- (30) Lu, Q.; Zhu, H. S.; Zhang, C. C.; Zhang, F.; Zhang, B.; Kaplan, D. L. *Biomacromolecules* **2012**, *13*, 826–832.
- (31) Greving, I.; Cai, M. Z.; Vollrath, F.; Schniepp, H. C. *Biomacromolecules* **2012**, *13*, 676–682.
- (32) Marcano, D. C.; Kosynkin, D. V.; Berlin, J. M.; Sinitskii, A.; Sun, Z. Z.; Slesarev, A.; Alemany, L. B.; Lu, W.; Tour, J. M. *ACS Nano* **2010**, *4*, 4806–4814.
- (33) Foo, C. W. P.; Bini, E.; Hensman, J.; Knight, D. P.; Lewis, R. V.; Kaplan, D. L. *Appl. Phys. A: Mater. Sci. Process.* **2006**, *82*, 223–233.
- (34) Dreyer, D. R.; Park, S.; Bielawski, C. W.; Ruoff, R. S. *Chem. Soc. Rev.* **2010**, *39*, 228–240.
- (35) Liu, J. B.; Fu, S. H.; Yuan, B.; Li, Y. L.; Deng, Z. X. *J. Am. Chem. Soc.* **2010**, *132*, 7279–7281.
- (36) Xu, S. J.; Yong, L.; Wu, P. Y. *ACS Appl. Mater. Interfaces* **2013**, *5*, 654–662.
- (37) Brown, C. P.; Harnagea, C.; Gill, H. S.; Price, A. J.; Traversa, E.; Licoccia, S.; Rosei, F. *ACS Nano* **2012**, *6*, 1961–1969.
- (38) Agnarsson, I.; Kuntner, M.; Blackledge, T. A. *PLoS One* **2010**, *5*, e11234.
- (39) Giesa, T.; Arslan, M.; Pugno, N. M.; Buehler, M. J. *Nano Lett.* **2011**, *11*, 5038–5046.
- (40) Adamcik, J.; Berquand, A.; Mezzenga, R. *Appl. Phys. Lett.* **2011**, *98*, 193701.
- (41) Adamcik, J.; Lara, C.; Usov, I.; Jeong, J. S.; Ruggeri, F. S.; Dietler, G.; Lashuel, H. A.; Hamley, I. W.; Mezzenga, R. *Nanoscale* **2012**, *4*, 4426–4429.
- (42) Knowles, T. P. J.; Buehler, M. J. *Nat. Nanotechnol.* **2011**, *6*, 469–479.
- (43) Mahmoudi, M.; Akhavan, O.; Ghavami, M.; Rezaee, F.; Ghiasi, S. M. A. *Nanoscale* **2012**, *4*, 7322–7325.
- (44) Bini, E.; Knight, D. P.; Kaplan, D. L. *J. Mol. Biol.* **2004**, *335*, 27–40.
- (45) Slotta, U.; Hess, S.; Spiess, K.; Stromer, T.; Serpell, L.; Scheibel, T. *Macromol. Biosci.* **2007**, *7*, 183–188.
- (46) Li, G. Y.; Zhou, P.; Shao, Z. Z.; Xie, X.; Chen, X.; Wang, H. H.; Chunyu, L. J.; Yu, T. Y. *Eur. J. Biochem.* **2001**, *268*, 6600–6606.

- (47) Lu, Q.; Hu, X.; Wang, X. Q.; Kluge, J. A.; Lu, S. Z.; Cebe, P.; Kaplan, D. L. *Acta Biomater.* **2010**, *6*, 1380–1387.
- (48) Dikin, D. A.; Stankovich, S.; Zimney, E. J.; Piner, R. D.; Dommett, G. H. B.; Evmenenko, G.; Nguyen, S. T.; Ruoff, R. S. *Nature* **2007**, *448*, 457–460.
- (49) Gao, J.; Liu, F.; Liu, Y. L.; Ma, N.; Wang, Z. Q.; Zhang, X. *Chem. Mater.* **2010**, *22*, 2213–2218.
- (50) Xu, Y. X.; Bai, H.; Lu, G. W.; Li, C.; Shi, G. Q. *J. Am. Chem. Soc.* **2008**, *130*, 5856–5857.
- (51) Li, C. X.; Bolisetty, S.; Mezzenga, R. *Adv. Mater.* **2013**, *25*, 3694–3700.